Clinics and Research in Hepatology and Gastroenterology 45 (2021) 101478

Available online at
ScienceDirect
www.sciencedirect.com

Elsevier Masson France
EM|consulte
www.em-consulte.com/en

CASE REPORT

Myxoid hepatocellular adenoma, a rare variant of hepatocellular adenoma with distinct imaging features: A case report with immunohistochemical and molecular analysis and literature review

Nicolas De Vos[a], Joni Van der Meulen[b], Malaïka Van Der Linden[c], Kathleen Claes[b], Ann-Sophie Candaele[c], Aude Vanlander[d], Roberto Ivan Troisi[e,1], Hans Van Vlierberghe[f], Peter Smeets[a], Jo Van Dorpe[c], Anne Hoorens[c,*]

[a] *Department of Radiology, Ghent University Hospital, Ghent 9000, Belgium*
[b] *Centre for Medical Genetics, Ghent University Hospital, Ghent 9000, Belgium*
[c] *Department of Pathology, Ghent University Hospital, Ghent 9000, Belgium*
[d] *Department of General Hepatobiliary and Liver Transplantation Surgery, Ghent University Hospital, Ghent 9000, Belgium*
[e] *Department of Human Structure and Repair, University of Ghent Faculty of Medicine, Ghent 9000, Belgium*
[f] *Department of Gastroenterology and Hepatology, Ghent University Hospital, Ghent 9000, Belgium*

Disponible sur Internet le 30 June 2020

KEYWORDS
Myxoid hepatocellular adenoma ;

Summary Preoperative imaging and histopathology, immunohistochemistry and molecular analysis after resection of 2 hepatocellular adenomas (HCAs) (20 and 2 cm) in a 53-year-old female patient were performed. On imaging, the large lesion resembled a myxoid HCA, while

* Corresponding author at: Department of Pathology, Ghent University Hospital, C.-Heymanslaan 10, 9000 Ghent, Belgium.
Adresses e-mail : nicolas.devos@uzgent.be (N. De Vos), joni.vandermeulen@ugent.be (J. Van der Meulen), malaika.vanderlinden@ugent.be (M. Van Der Linden), kathleen.claes@ugent.be (K. Claes), ann-sophie.candaele@uzgent.be (A.-S. Candaele), aude.vanlander@uzgent.be (A. Vanlander), roberto.troisi@ugent.be (R.I. Troisi), hans.vanvlierberghe@uzgent.be (H. Van Vlierberghe), peter.smeets@ugent.be (P. Smeets), jo.vandorpe@uzgent.be (J. Van Dorpe), anne.hoorens@uzgent.be, anne.hoorens@ugent.be (A. Hoorens).
[1] Department of Clinical Medicine and Surgery, ''Federico IIÜniversity, Naples, 80138, Italy.

https://doi.org/10.1016/j.clinre.2020.06.004

HNF1A mutated hepatocellular adenoma ;
Sonic hedgehog hepatocellular adenoma ;
PTGDS ;
ASS1+ hepatocellular adenoma

the small lesion resembled a more conventional HCA with a small myxoid/fluid area. On microscopy, the large lesion showed cords and nests of hepatocytes embedded in abundant myxoid matrix, while the small lesion resembled a conventional HCA with small foci of myxoid change and serosities; both consistent with a myxoid HCA. Immunophenotyping and molecular subtyping excluded inflammatory HCA, CTNNB1 mutated HCA and sonic hedgehog HCA, and was consistent with *HNF1A* mutated HCA. The myxoid change as well as the serosities may allow imaging diagnosis of myxoid HCA. As fluid vacuoles can also be present in ASS1 + HCA, sonic hedgehog HCA has to be considered in the differential diagnosis.

Introduction

Molecular classification divided hepatocellular adenoma (HCA) into different subtypes, based on inactivating mutations in hepatocyte nuclear factor 1A (*HNF1A*), activations of inflammatory signalling pathways, activating mutations in ß-catenin (CTNNB1) or activation of sonic hedgehog pathway [1,2]. Myxoid HCA is a rare HCA variant, characterised by the presence of prominent myxoid stroma [3—5]. It remains controversial whether it is specific for a known HCA subtype [4—6]. Sonic hedgehog HCA (shHCA) is a recently described new subtype of HCA with genomic fusion between inhibin beta E subunit (*INHBE*) and *GLI* family zinc finger 1 (*GLI1*), leading to overexpression of GLI1, a transcription factor controlling sonic hedgehog pathway activation [1]. Prostaglandin D synthase (PTGDS)/argininosuccinate synthase 1 (ASS1) overexpression by immunohistochemistry was suggested to be a reliable surrogate marker of shHCA [1,7—9]. These lesions have a high risk of bleeding [1,7]. There are no typical features allowing accurate non-invasive diagnosis of shHCA on imaging. ASS1 positive HCA (ASS1 + HCA) is a subtype of HCA, similar if not identical to shHCA [8]. ASS1 + HCA shows fluid vacuoles and serosities, leading to the presence of peculiar fluid vacuoles on imaging [8,10].

We report a patient with two myxoid HCAs. Imaging features, histological characteristics, immunohistochemical profile and molecular analysis are described.

This study was approved by the Medical Ethics Committee of Ghent University Hospital, and written informed consent was obtained from the patient.

Material and methods

Histopathology and Immunohistochemistry

The specimen was routinely processed for light microscopy. On selected blocks picrosirius red, reticulin and Alcian blue staining (pH 2.5) was performed per lab protocol. Masson's trichrome, Periodic Acid-Schiff (PAS), PAS with diastase and Perls staining was performed on the BenchMark Special Stains platform (Ventana; Roche, Tuscon, AZ). A panel of antigens was applied to selected paraffin blocks using an automated immunostainer (BenchMark XT Ventana) with appropriate controls. The panel of immunohistochemical stains included HepPar1 (OCH1E5, Agilent, Santa Clara, CA, 1/600), arginase-1 (ABS535, Merck KGaA, Darmstadt, Germany, 1/3000), CK7 (SP52, Ventana, RTU), GS (glutamine synthetase, Clone 6, BD Transduction Laboratories, BD Biosciences, San Jose, CA, 1/1500), β-catenin (Beta-catenin, Clone 14, Ventana, RTU), LFABP (liver fatty acid binding protein, L2B10, Abcam, Cambridge, UK, 1/800), CRP (C-reactive protein, Y284, Abcam, 1/800), SAA (serum amyloid A, mc1, Agilent, Santa Clara, CA, 1/1000), ASS1 (argininosuccinate synthase 1, HPA020896, Sigma-Aldrich, St. Louis, MO, 1/1000), PTGDS (prostaglandin D synthase, HPA004938, Sigma-Aldrich, St. Louis, MO, 1/25), glypican 3 (GC33, Ventana, RTU), HSP 70 (heat shock protein 70, W27, Santa Cruz Biotechnology, Santa Cruz, CA, 1/100), and alpha-fetoprotein (polyclonal, Agilent, 1/200).

Case presentation

A 53-year-old woman presented with a large liver mass, an incidental finding on CT after trauma. It was located in the left liver lobe and had a maximal diameter of 20 cm. In addition, a smaller lesion was observed in liver segment VI. She had no significant past medical history. She had taken oral contraceptives for many years.

On MRI (Fig. 1), the large lesion in the left liver lobe was markedly hyperintense with interspersed bands of lower signal intensity on T2-weighted imaging (T2-WI). On T1-weighted imaging (T1-WI), the lesion was markedly hypointense. After intravenous administration of the hepatocyte-specific gadolinium contrast agent gadobenic acid (Gd-BOPTA), the lesion demonstrated heterogeneous, centripetal-predominant arterial enhancement and progressive and more homogeneous enhancement during later phases. During hepatobiliary phase imaging, the lesion showed no contrast retention, indicating absence of normally functioning hepatocytes and/or bile ducts. These findings are compatible with a myxoid hepatocellular neoplasm. It may be difficult to distinguish this lesion from a giant cavernous hemangioma. However, the classic peripheral discontinuous globular enhancement with progressive centripetal filling in giant cavernous hemangioma is different from the more heterogeneous and progressive enhancement seen in a myxoid hepatic neoplasm [5]. The small

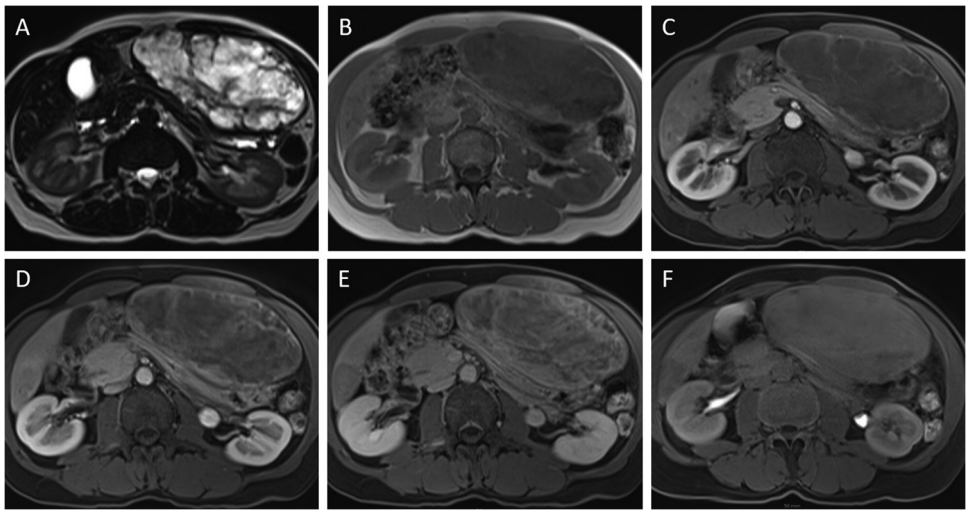

Figure 1 Axial MRI confirms both lesions. A. On T2-weighted imaging, the left-sided lesion demonstrates marked hyperintensity with interspersed bands of lower signal intensity, while the right-sided lesion is discretely hyperintense to the adjacent liver parenchyma, with a central punctiform area of marked hyperintensity. B. On T1-weighted imaging, the left-sided lesion is markedly hypointense, while the right-sided lesion is discretely hypointense to the surrounding liver parenchyma, with a central punctiform area of marked hypointensity. C—E. Arterial, portal venous and delayed phase dynamic contrast-enhanced fat-saturated T1-weighted images with gadobenic acid (Gd-BOPTA) demonstrate heterogeneous, centripetal-predominant arterial enhancement that progressively and more homogeneously enhances on later phases in the left-sided lesion. The right-sided lesion remains hypointense to normal liver parenchyma in all phase, with progressive enhancement of the central punctiform area. F. 90-minute hepatobiliary phase image demonstrates absence of contrast retention within the lesions, indicating absence of normally functioning hepatocytes and/or bile ducts.

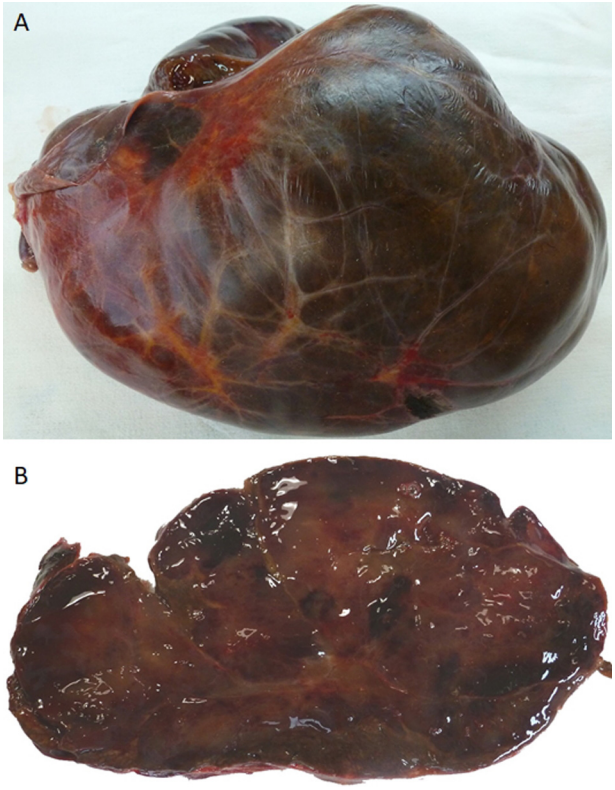

Figure 2 Left lobectomy specimen. A. A whitish red large liver mass is visible through the liver capsule. B. On cutting a liver mass with a diameter of 20 cm is observed, displaying cystic sticky mucoid areas, alternating with small fibrotic and hemorrhagic areas.

lesion in the right liver lobe was discretely hyperintense to the adjacent liver parenchyma on T2-WI, with a central punctiform area of marked hyperintensity. On T1-WI, the lesion was discretely hypointense, with a central area of marked hypointensity. After administration of Gd-BOPTA, the lesion enhanced slightly less than normal liver parenchyma in all phases, except for the central punctiform area, which showed progressive enhancement. During hepatobiliary phase imaging, the lesion showed no contrast retention. These findings are compatible with a hepatocellular adenoma with a central punctiform myxoid component. This lesion may be difficult to distinguish from focal nodular hyperplasia (FNH) with a central scar. The lack of contrast retention during hepatobiliary phase imaging, however, is atypical for FNH [5].

Hand-assisted laparoscopic left lobectomy was performed, in combination with resection of the lesion in segment VI. Grossly, a whitish red large liver mass of 20 cm diameter was observed through the liver capsule in the left lobectomy specimen (Fig. 2A). It was sharply delineated and showed cystic sticky mucoid areas alternating with hemorrhagic areas (Fig. 2B). The resection of segment VI contained an irregularly delineated mass of 2 cm diameter, slightly paler in colour than the surrounding parenchyma. Microscopically, the large tumour predominantly consisted of cords and small clusters of monotonous bland appearing polygonal cells with vesicular nuclei with small nucleoli, embedded in an abundant myxoid/mucoid matrix (Fig. 3A). The cytoplasm of the tumour cells was granular eosinophilic and contained abundant lipofuscin granules (Fig. 3B). Hemorrhagic areas were present, as well as few fibrous septa (Fig. 3C). The myxoid/mucoid matrix was lightly Alcian blue positive

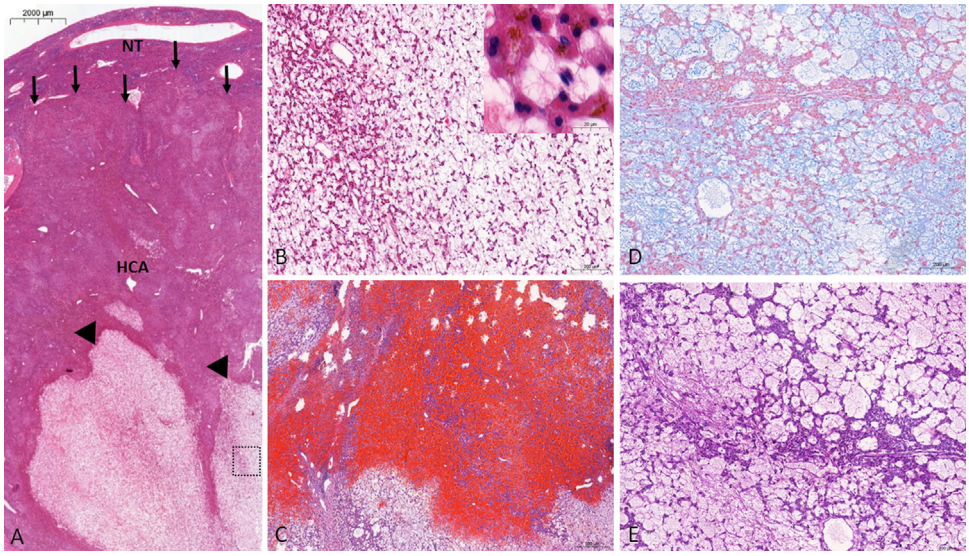

Figure 3 Histopathology large tumour. A. The tumour predominantly consists of cords and small clusters of cells embedded in an abundant myxoid/mucoid matrix (arrowheads) with at the periphery of the tumour solid areas of neoplastic cells; arrows indicate the limits between HCA and non-tumoural liver (NT). B. Higher magnification of the area marked with a rectangle in A. The cytoplasm of the tumour cells is granular eosinophilic and contains abundant lipofuscin granules (inset). C. Hemorrhagic areas are present. D. The myxoid/mucoid matrix is lightly Alcian blue positive. E. and weakly PAS diastase positive.

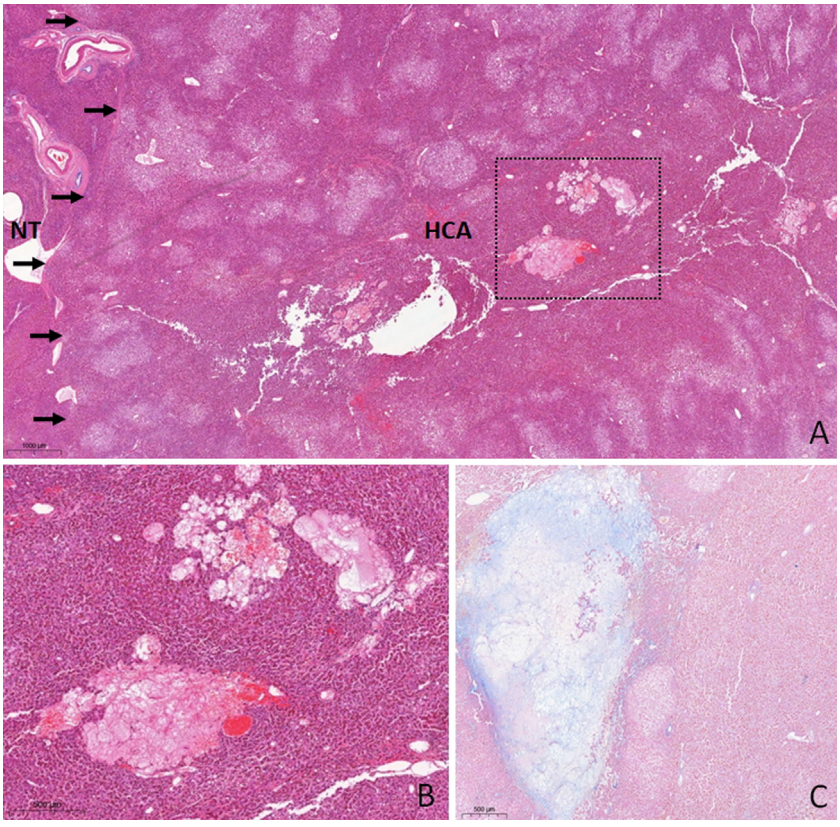

Figure 4 Histopathology small tumour. A. The tumour consists of normal appearing hepatocytes arranged in cords, with small foci of myxoid/mucoid stroma and serosities; arrows indicate the limits between HCA and non-tumoural liver (NT). B. Higher magnification of the area marked with a rectangle in A showing small foci of myxoid/mucoid stroma and serosities. C. Foci of myxoid/mucoid stroma are lightly Alcian blue positive.

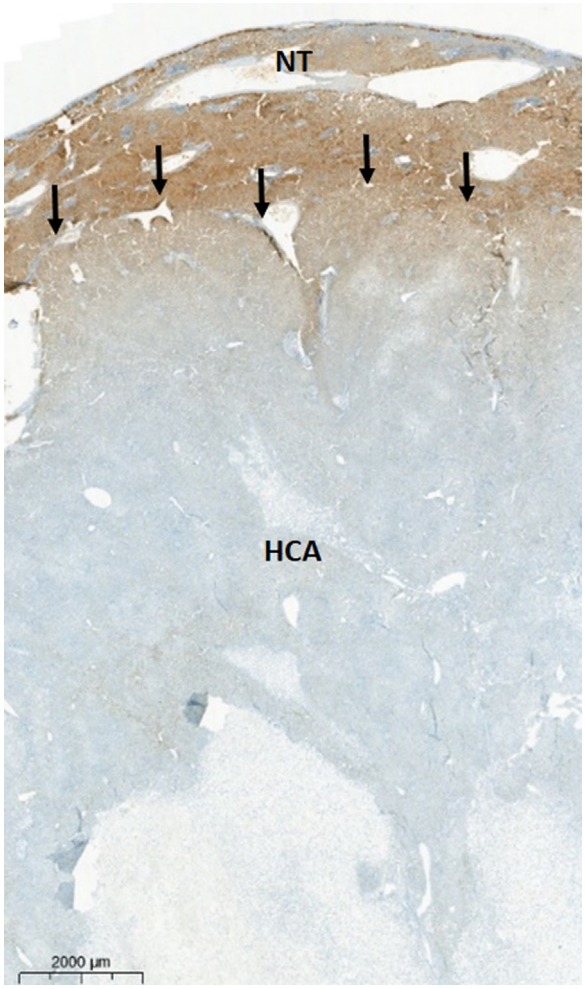

Figure 5 LFABP staining large tumour. The tumour (HCA) shows a peripheral narrow rim of cells with weak LFABP staining in comparison with the surrounding non-tumoural liver parenchyma (NT), gradually diminishing towards the centre of the lesion and becoming completely negative; arrows indicate the limits between HCA and non-tumoural liver (NT).

(Fig. 3D) and weakly PAS diastase positive (Fig. 3E). No intracellular mucin was observed. Focally, predominantly at the periphery of the lesion, solid nests of neoplastic cells resembling normal hepatocytes were observed, surrounding large, predominantly thin-walled vessels. The lesion in addition contained numerous small unpaired arteries. The smaller lesion consisted of normal appearing hepatocytes arranged in cords, with focal sinusoidal dilatation and peliosis, and small foci of similar appearing myxoid/mucoid stroma and serosities (Fig. 4A—C). In this lesion too, hepatocytes contained numerous lipofuscin granules. Both lesions lacked portal tracts and showed mild steatosis. The surrounding non-tumoural liver parenchyma appeared unremarkable. In both lesions, the tumour cells were positive for HepPar1 and arginase-1. Few tumour cells were CK7 positive, but there was no positivity for CK19. Both tumours displayed a peripheral narrow rim of cells with weak LFABP (liver fatty acid binding protein) staining, gradually diminishing towards the centre of the lesions and becoming completely negative (Fig. 5), whereas LFABP was normally expressed in the surrounding liver parenchyma. The tumours were negative for SAA (serum amyloid A) and CRP (C-reactive protein). There was no increased staining for GS (glutamine synthetase) and no nuclear accumulation of β-catenin. PTGDS (prostaglandin D synthase) staining at low power view appeared heterogeneous due to myxoid areas, but was clearly overexpressed in both lesions, compared to the surrounding liver parenchyma. At higher magnification, the labelling was however coarsely granular, corresponding to strong aspecific staining of lipofuscin granules, but not a diffuse cytoplasmic staining (Fig. 6A—D). ASS1 (argininosuccinate synthase 1) staining showed diffuse expression in both lesions, contrasting with normal expression with zonation in non-tumoural liver. Due to steatotic areas, the staining appeared focally heterogeneous with weakly stained areas alternating with darker stained areas. However, at low magnification, no overall higher intensity than the zonated staining in the non-tumoural liver was observed (Fig. 7A and B). There was no loss of reticulin and the lesions did not display positivity for glypican 3, HSP70 (heat shock protein 70) or alpha-fetoprotein.

Tumoural DNA was extracted from formalin-fixed, paraffin-embedded (FFPE) sections after macrodissection. Targeted next-generation sequencing was performed with a 69 gene panel including *AKT1, ALK, APC, AR, BAP1, BRAF, BRCA1, BRCA2, CCND1, CDK4, CDK6, CDKN2A, CDKN2B,*

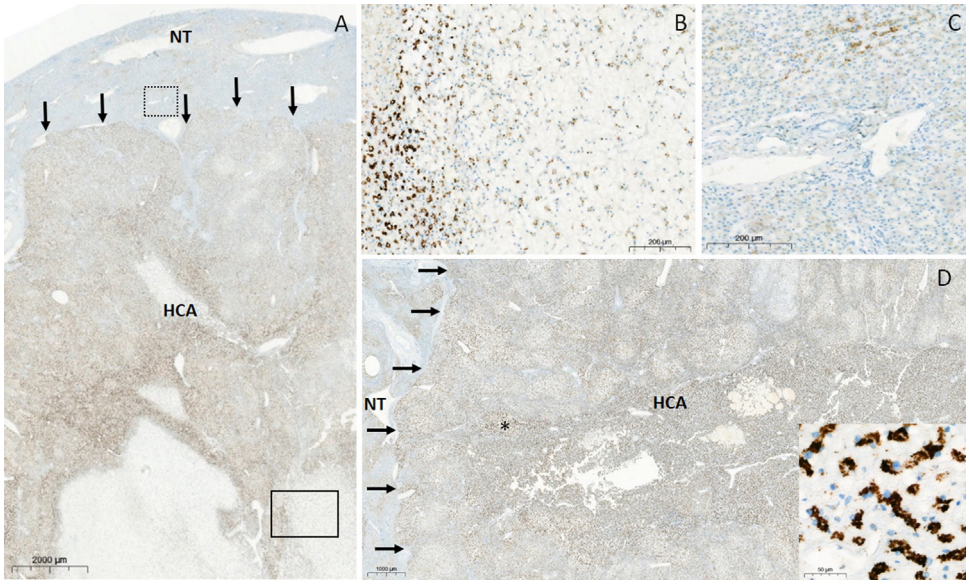

Figure 6 PTGDS immunohistochemistry. A. The large tumour (HCA) shows clear overexpression compared to the surrounding non-tumoural liver parenchyma (NT); arrows indicate the limits between HCA and non-tumoural liver (NT). B. Higher magnification of the area marked with a rectangle with full line in A showing positive tumour cells. C. Higher magnification of the area marked with a rectangle with dashed line in A showing no labelling in periportal hepatocytes and lipofuscin granules in centrilobular hepatocytes in non-tumoural liver. D. Similar staining for PTGDS is observed in the smaller lesion; arrows indicate the limits between HCA and non-tumoural liver (NT). Inset shows higher magnification of the area indicated with an asterisk: Tumoural cells show strong coarsely granular staining suggestive of aspecific labelling of lipofuchsin granules, which are much more abundant in the tumour compared to the non-tumoural liver.

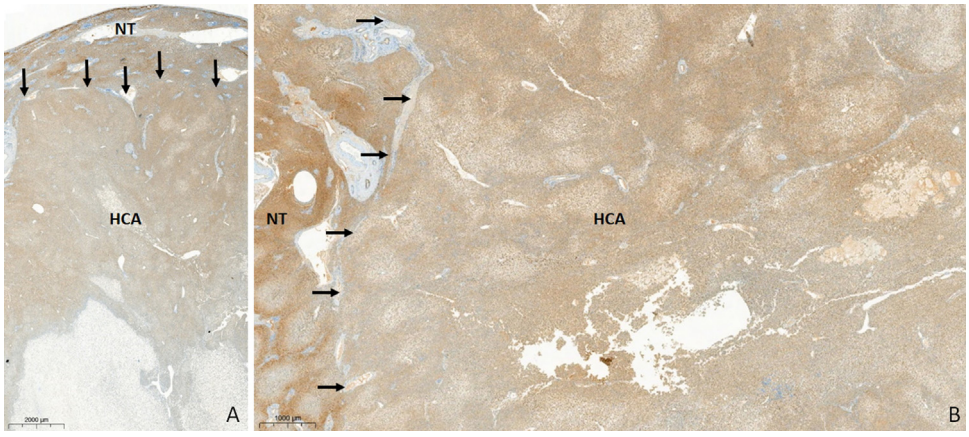

Figure 7 ASS1 immunohistochemistry. A. Large lesion. B. Small lesion. Both tumours (HCA) show diffuse expression, without zonation, but there is no overall higher intensity than the zonated staining in the non-tumoural liver; arrows indicate the limits between HCA and non-tumoural liver (NT).

CTNNB1, DDR2, DICER1, DPYD, EGFR, ERBB2, ERBB3, ERBB4, ESR1, FBXW7, FGFR1, FGFR2, FGFR3, FOXL2, FRK, GATA3, GNA11, GNAQ, GNAS, H3F3A, H3F3B, HIST1B3, HIST1H3C, HNF1A, HRAS, IDH1, IDH2, IL6ST, JAK1, JAK2, KIT, KRAS, MAP2K1, MET, NRAS, NTRK1, NTRK3, PDGFRA, PIK3CA, PIK3R1, POLE, PTEN, RB1, RET, RNF43, ROS1, SMAD4, SMARCA4, SMARCB1, SMO, SPOP, STAT3, STK11, TERT, TP53 and *VHL* (Roche, Basel, Switzerland). This panel encompasses genes characteristic for beta-catenin mutated HCA (*CTNNB1* exon 2, 3, 4, 7, 8/NM_001904.4/build hg38), for inflammatory HCA (*GNAS* exon 7, 8, 9/NM_000516.5/build hg38, *JAK1* exon 15, 16/NM_002227.4/build hg38, *FRK* exon 6/NM_002031.3/build hg38, *STAT3* exon 3, 6, 17, 20, 21/NM_139276.2/build hg38, *IL6ST* exon 6, 10/NM_002184.3/build hg38), for *HNF1A* mutated HCA (*HNF1A* all exons/NM_000545.6/build hg38) and for malignant transformation in HCA (*TERT* promoter region/NM_198253.2/build hg38). None of the tumours displayed a *CTNNB1* mutation in exon 2, 3, 4, 7 or 8, consistent with the absence of nuclear ß-catenin staining and absence of overexpression of GS in immunohistochemistry [11]. In addition, no *TERT* mutation was detected in both tumour samples. Molecular analysis did not reveal arguments for inflammatory HCA as no activating mutations

were observed in *GNAS*, *JAK1*, *FRK*, *STAT3* or *IL6ST*, consistent with the lack of overexpression of CRP and SAA in immunohistochemistry [11]. In the large lesion (tumour cell percentage 80%), a variant was found in *HNF1A* gene: *HNF1A* c.824_833del p.(Glu275Glyfs*64) at 36% variant allele frequency (VAF). The smaller lesion (tumour cell percentage 80%) harboured a different *HNF1A* variant: *HNF1A* c.793T > G [p.(Tyr265Asp)] 36% VAF. There was no bi-allelic variant detected in *HNF1A*. In addition, in both lesions, the same variant was found in Discoidin Domain Receptor Tyrosine Kinase 2 gene: *DDR2* c.861C > G [p.(His287Gln)] 50% VAF and 49% VAF, respectively in the large lesion and in the smaller lesion. In parallel, copy number aberration (CNA) detection by copy number variation sequencing (CNV-seq) was performed on FFPE tumour tissue [12]. This showed a 450 kb duplication in chromosome band 14q21.2 in both lesions. This region, however, does not contain known genes. In addition, a chromosome-5 duplication could be detected in the smallest lesion only. However, sample quality and quantity of the largest lesion was lower, resulting in a higher level of noise in the copy number profile and hindering identifying CNAs. Of all the genes actually known to be linked to hepatocellular adenomas, only one, *IL6ST* linked to inflammatory HCA, is localised on chromosome 5. As already emphasised, inflammatory HCA could be excluded because of lack of overexpression of CRP and SAA in immunohistochemistry [11].

Imaging, histology and immunohistochemistry of both liver tumours are suggestive of HCAs with myxoid component. The large lesion in the left liver lobe displayed prominent characteristics of myxoid HCA [3—6]. The small lesion in the right liver lobe resembled more conventional type HCA, with focal prominent sinusoidal dilatation and peliosis; however, displaying in addition small foci of myxoid change and serosities [3—6]. The serosities observed in the small lesion appear identical to those described in ASS1 + HCA [8,10]. There was, however, no overexpression of ASS1 compared to surrounding non-tumoural periportal hepatocytes and only aspecific labelling for PTGDS, making the diagnosis of shHCA unlikely [7]. Molecular analysis and immunophenotyping, with mutation of *HNF1A* and diminished LFABP staining, are compatible with *HNF1A* mutated HCA (HHCA).

The patient is regularly followed-up, including imaging, and is without evidence of local disease recurrence or metastases 24 months following surgery.

Discussion

Only very few cases of myxoid HCA have been reported in the literature to date (Table 1). Almost all cases presented with multiple adenomas, and the myxoid change was often present, at least focally, in multiple adenomas [3—5,13]. Myxoid HCA is not a HCA subtype, but a variant, probably not specific to one of the HCA subtypes. It is described in the latest edition of the WHO Classification of Digestive Tumours under the chapter of *HNF1A* inactivated HCA (HHCA) as a rare feature of this subtype of HCA. In all cases reported in the literature until now, where immunophenotyping and/or molecular subtyping were performed, myxoid adenomas were characterised by loss of LFABP expression and/or *HNF1A* mutation [4,6,13]. In our patient, both tumours showed weak LFABP expression at the periphery of the lesions, gradually decreasing towards the centre and becoming completely negative. This staining pattern appears different from the totally absent staining that is usually shown in *HNF1A* mutated HCA (HHCA) and is also not mentioned in other myxoid HCAs. Decreased LFABP staining in HCA has been previously mentioned in some shHCA, a subtype of HCA with a high risk of severe bleeding, although it appears to be diffuse weak labelling, different from what is observed in the present case [7—9]. In both tumours of our patient, a mono-allelic variant in the *HNF1A* gene was observed. Similarly, Torbenson et al. reported heterozygous mutations in *HNF1A* in the myxoid adenomas from the Mayo clinic [6]. Hypothetically, mono-allelic variants might be a possible explanation for the reduced staining for LFABP in both tumours. In that case, we would, however, expect diffuse reduced staining and the hypothesis of a relationship with reduced LFABP staining thus remains questionable. Moreover, a mono-allelic variant of *HNF1A* has not been described in shHCA. *HNF1A* inactivation in HHCA is often bi-allelic, but mono-allelic mutations in combination with LOH have also been described. LOH can remain undetected in NGS and CNVseq analysis. Peripheral staining of the tumours may result from antigen diffusion from the surrounding non-tumoural liver parenchyma, leading to erroneous conclusion of diminished staining, instead of loss of LFABP expression. Antigen diffusion is a possible pitfall in immunohistochemistry, usually resulting from delayed fixation.

The characteristic prominent myxoid change in the large lesion allows accurate non-invasive diagnosis as myxoid hepatocellular neoplasm on imaging [5]. The myxoid matrix might be the result of degeneration of clotted blood in peliotic cysts and hemorrhagic areas. Moreover, collagenous cell-poor zones were also present, as well as some dense fibrotic bands. In giant cavernous hemangiomas, similar areas of hypocellular myxoid tissue can be observed, thought to represent an intermediate stage in the evolution from thrombosis within the vascular channels to final well-formed fibrous scars [14]. The frequent presence of these myxoid cysts in giant cell hemangioma may contribute to the misinterpretation of myxoid HCA with prominent myxoid change as giant cell hemangioma on imaging [15]. Also, in our case, the large lesion in the left liver lobe was initially considered a giant cavernous hemangioma on MRI, while the small lesion in the right liver lobe was thought to be suggestive of a HCA. Histologically, distinction of myxoid HCA from hemangioma is straightforward, but differentiation from mucin-producing cholangiocarcinoma may be challenging. Positivity for the hepatocyte markers HepPar1 and arginase-1 and negative staining for the cholangiocyte maker CK19 allow to avoid misdiagnosis.

The small myxoid HCA in our patient not only showed small foci of myxoid change, but also fluid vacuoles and serosities identical to those reported in ASS1 + HCA, similar, if not identical, to shHCA [10]. It remains unknown why these fluid vacuoles and serosities, which are very frequent in ASS1 + HCA, even when the tumours are small, lead to severe bleeding in shHCA, while they appear to evolve into myxoid foci in myxoid HCA. Both tumours in our patient showed a mutation in *DDR2*. As *DDR2* is involved in remodelling of the extracellular matrix, it might be implicated in development

Table 1 Characteristics of patients with myxoid HCA reported in the literature, including the present case.

Number of tumours	Diameter of largest tumour	M/F	Age at diagnosis	Miscellaneous conditions[a]	Malignant transformation	Reference
1	16 cm	M	26	No	HCA with HCC focus[b]	Galassi A et al. [3]
6	4 cm	M	34	No	HCA	Salaria SN et al. [4]
6	9 cm	M	45	No	HCA	Salaria SN et al. [4]
> 10	17.5 cm	M	20	No	HCA	Salaria SN et al. [4]
5	14.5 cm	F	65	No	HCA	Salaria SN et al. [4]
12	11.5 cm	M	45	No	HCA	Young JT et al. [5]
1	7 cm	M	52	Overweight Hormone replacement therapy	HCA with subsequent malignant transformation	Young JT et al. [5]
1[c]	12 cm	F	52	Possible Osler—Weber—Rendu syndrome	Malignant transformation	Putra J et al. [13]
> 10[c]	8.5 cm	M	27	Teralogy of Fallot	Malignant transformation	Putra J et al. [13]
> 10	8 cm	F	53	No	Malignant transformation	Putra J et al. [13]
> 10[c]	7 cm	F	55	Budd—Chiari syndrome	Malignant transformation	Putra J et al. [13]
1[c]	10 cm	F	64	No	Malignant transformation	Putra J et al. [13]
2	20 cm	F	53	Oral contraceptive use	HCA	Present case

[a] Oral contraceptive use, hormone replacement therapy or anabolic steroid use, diabetes, overweight, steatohepatitis or fibrosis of non-tumoural liver, other underlying chronic liver disease.
[b] Focal reticulin loss.
[c] Only focal myxoid change is reported (defined as < 50%). All other cases show in at least one lesion predominant myxoid features.

of the prominent myxoid stroma [16]. This also remains hypothetical, as *DDR2* mutation has not yet been investigated in other myxoid HCA. The fluid vacuoles and serosities may, in addition to the myxoid change, allow imaging diagnosis of myxoid HCA. As fluid vacuoles can also be present in ASS1 + HCA, shHCA has to be considered in the differential diagnosis [8,10]. This case emphasises the importance of correctly interpreting immunohistochemical stainings to avoid pitfalls in the diagnosis of shHCA. PTGDS/ASS1 overexpression by immunohistochemistry was suggested to be a reliable surrogate marker of shHCA [1,7—9]. Binding of PTGDS antibodies to lipofuscin granules, however, can be misleading and should not be confused with true diffuse cytoplasmic PTGDS staining. Concerning ASS1 immunohistochemistry, not only positivity, but overexpression of ASS1 in the tumour in comparison to the non-tumoural liver, is mandatory for the diagnosis of shHCA [8].

Drawing general conclusions based on the few reported cases in literature is not possible, but preliminary observations suggest that HCA with myxoid features is more common in males and is less related to obesity and diabetes (Table 1) [1]. Seven of the thirteen reported cases of myxoid HCA showed malignant transformation (Table 1). Five cases of HCA with myxoid features showing malignant transformation were *HNF1A* mutated adenomas (in 2 of these cases, inactivating mutations of *HNF1A* were demonstrated, while classification in the 3 other cases was based on immunohistochemical subtyping). The high percentage of malignant transformation in the reported cases of myxoid HCA, however not necessary, should be linked to inherent molecular characteristics of the lesion, but may be related to male gender, which is associated with a higher risk for malignant transformation of HCA at baseline, independent of molecular classification. Also, the large tumour size might be implicated in the high percentage of malignant transformation. As differentiation between benign and malignant myxoid hepatocellular neoplasms is not possible on imaging, these lesions should be referred for surgery [5]. In addition, follow-up after surgery is required, as most patients with myxoid HCA have more than one lesion [4—6,16].

Conclusions

Immunophenotyping and molecular subtyping of two myxoid HCAs (20 and 2 cm) excluded inflammatory HCA, CTNNB1 mutated HCA and sonic hedgehog HCA and was consistent with *HNF1A* mutated HCA. Remarkably, next to small myxoid foci, fluid vacuoles and serosities were observed, similar to the fluid vacuoles resulting from degeneration of clotted blood described in ASS1 + HCA. Development of new techniques for molecular subtyping, including detection of genetic fusions and small chromosomal deletions as well as proteomic analysis for biomarker quantification on FFPE tissue, can contribute to further clarification of similarities and differences between myxoid HCA and ASS1 + HCA/shHCA and

may explain why these fluid vacuoles and serosities lead to severe bleeding in shHCA, while they appear to evolve into myxoid foci in myxoid HCA. The myxoid change as well as the serosities may allow imaging diagnosis of myxoid HCA. As fluid vacuoles can also be present in ASS1 + HCA, shHCA has to be considered in the differential diagnosis.

Funding

This research did not receive any specific grant from funding agencies in the public, commercial, or not-for-profit sectors.

Author contributions

Nicolas De Vos analysed and interpreted the imaging findings, reviewed the literature and contributed to manuscript drafting; Joni Van der Meulen, Malaïka Van Der Linden and Kathleen Claes performed and interpreted the molecular analysis and Joni Van der Meulen and Malaïka Van Der Linden contributed to manuscript drafting; Ann-Sophie Candaele performed the macroscopic analysis of the resection specimen; Aude Vanlander and Roberto Ivan Troisi were the patient's surgeons and are involved in follow-up; Hans Van Vlierberghe is involved in follow-up, Peter Smeets analysed and interpreted the imaging findings; Jo Van Dorpe contributed to conception and design of the study, Anne Hoorens performed the macroscopy and microscopy of the resection specimen, reviewed the literature and contributed to manuscript drafting. All authors were responsible for the revision of the manuscript for important intellectual content and issued final approval for the version submitted.

Disclosure of interest

The authors declare that they have no competing interest.

Références

[1] Nault JC, Couchy G, Balabaud C, Morcrette G, Caruso S, Blanc JF, et al. Molecular classification of hepatocellular adenoma associates with risk factors, bleeding, and malignant transformation. Gastroenterology 2017;152:880—94, http://dx.doi.org/10.1053/j.gastro.2016.11.042.

[2] Nault JC, Paradis V, Cherqui D, Vilgrain V, Zucman-Rossi J. Molecular classification of hepatocellular adenoma in clinical practice. J Hepatol 2017;67:1074—83, http://dx.doi.org/10.1016/j.jhep.2017.07.009.

[3] Galassi A, Pasquinelle G, Guerini A, Martinelli G, Venza E. Benign myxoid hepatocellular tumour: a variant of liver-cell adenoma. Liver 1995;15:233—5, http://dx.doi.org/10.1111/j.1600-0676.1995.tb00677.x.

[4] Salaria SN, Graham RP, Aishima S, Mounajjed T, Yeh MM, Torbenson MS. Primary hepatic tumours with myxoid change: morphologically unique hepatic adenomas and hepatocellular carcinomas. Am J Surg Pathol 2015;39:318—24, http://dx.doi.org/10.1097/PAS.0000000000000382.

[5] Young JT, Kurup AN, Graham RP, Torbenson MS, Venkatesh SK. Myxoid hepatocellular neoplasms: imaging appearance of a unique mucinous tumour variant. Abdom Radiol (NY) 2016;41:2115—22, http://dx.doi.org/10.1007/s00261-016-0812-x.

[6] Torbenson M. Hepatic adenomas: classification, controversies, and consensus. Surg Pathol Clin 2018;11:351—66, http://dx.doi.org/10.1016/j.path.2018.02.007.

[7] Henriet E, Abou Hammoud A, Dupuy JW, Dartigues B, Ezzoukry Z, Dugot-Senant N, et al. Argininosuccinate synthase 1 (ASS1): a marker of unclassified hepatocellular adenoma and high bleeding risk. Hepatology 2017;66:2016—28, http://dx.doi.org/10.1002/hep.29336.

[8] Bioulac-Sage P, Sempoux C, Frulio N, Le Bail B, Blanc JF, Castain C, et al. Snapshot summary of diagnosis and management of hepatocellular adenoma subtypes. Clin Res Hepatol Gastroenterol 2019;43:12—9, http://dx.doi.org/10.1016/j.clinre.2018.07.007.

[9] Nault JC, Couchy G, Caruso S, Meunier L, Caruana L, Letouzé E, et al. Argininosuccinate synthase 1 and periportal gene expression in sonic hedgehog hepatocellular adenomas. Hepatology 2018;68:964—76, http://dx.doi.org/10.1002/hep.29884.

[10] Frulio N, Balabaud C, Laurent C, Trillaud H, Bioulac-Sage P. Unclassified hepatocellular adenoma expressing ASS1 associated with inflammatory hepatocellular adenomas. Clin Res Hepatol Gastroenterol 2019;43:e63—7, http://dx.doi.org/10.1016/j.clinre.2019.03.012.

[11] Bioulac-Sage P, Cubel G, Balabaud C, Zucman-Rossi J. Revisiting the pathology of resected benign hepatocellular nodules using new immunohistochemical markers. Semin Liver Dis 2011;31:91—103, http://dx.doi.org/10.1055/s-0031-1272837.

[12] Van der Linden M, Raman L, Vander Trappen A, Dheedene A, De Smet M, Sante T, et al. Detection of copy number alterations by shallow whole genome sequencing of formalin-fixed paraffin-embedded tumour tissue. Arch Pathol Lab Med 2019, http://dx.doi.org/10.5858/arpa.2019-0010-OA [Epub ahead of print].

[13] Putra J, Ferrell LD, Gouw ASH, Paradis V, Rishi A, Sempoux C, et al. Malignant transformation of liver fatty acid binding protein-deficient hepatocellular adenomas: histopathologic spectrum of a rare phenomenon. Mod Pathol 2019, http://dx.doi.org/10.1038/s41379-019-0374-x [Epub ahead of print].

[14] Kim JM, Chung WJ, Jang BK, Hwang JS, Kim YH, Kwon JH, et al. Hemorrhagic hemangioma in the liver: a case report. World J Gastroenterol 2015;21:7326—30, http://dx.doi.org/10.3748/wjg.v21.i23.7326.

[15] Danet IM, Semelka RC, Braga L, Armao D, Woosley JT. Giant hemangioma of the liver: MR imaging characteristics in 24 patients. Magn Reson Imaging 2003;21:95—101, http://dx.doi.org/10.1016/s0730-725x(02)00641-0.

[16] Blissett AR, Garbellini D, Calomeni EP, Mihai C, Elton TS, Agarwal G. Regulation of collagen fibrillogenesis by cell-surface expression of kinase dead DDR2. J Mol Biol 2009;385:902—11, http://dx.doi.org/10.1016/j.jmb.2008.10.060.